A7RC Peptide Modified Paclitaxel Liposomes Dually Target Breast Cancer

A7RC Peptide Modified Paclitaxel Liposomes Dually Target Breast Cancer

Jingyan Cao[1], Ran Wang[2], Ning Gao[2, 3], Minghui Li[2], Xuyu Tian[2,5], Weili Yang[2], Ying Ruan[2], Chunlan Zhou[2], Guangtian Wang[2], Xiaoying Liu[2], Shukun Tang[2], Yan Yu[1], Ying Liu[1], Guangyu Sun[1], Haisheng Peng[2,4,*], and Qun Wang[4,*]

[1]*Department of Medical Oncology, The Tumor Hospital of Harbin Medical University, 150 Hapin Road, Harbin, 150086, China*

[2] *Department of Pharmaceutics, Daqing Campus, Harbin Medical University, 1 Xin Yang Road Daqing, 163319, China*

[3] *Department of Pharmaceutics, Harbin Commercial University, 138 Tong Da Street Harbin, 150076, China*

[4]*Department of Chemical and Biological Engineering, Iowa State University, Ames, IA 50011, United States*

[5]*Department of NMR, Daqing Oilfield General Hospital, 9 Zhong Kang Road Daqing, 163319, China*

* Corresponding author:

Haisheng Peng, Ph. D.

Department of Pharmaceutics
Daqing Campus of Harbin Medical University
1 Xinyang Rd Daqing, 163319, China
Tel: +86-459-8153 003
Fax: +86-459-8977 588
E-mail: fisher1688@163.com

Qun Wang, Ph. D.

Department of Chemical and Biological Engineering
Iowa State University
2114 Sweeney Hall
Ames, Iowa 50011
Office: (515) 294-4218
Fax: (515) 294-8216
E-mail: qunwang@iastate.edu

Abstract: A7R peptide (ATWLPPR), a ligand of NRP-1 receptor, regulates the intracellular signal transduction related to tumor vascularization and tumor growth. Here, we designed A7R-cysteine peptide (A7RC) surface modified paclitaxel liposomes (A7RC-LIPs) to achieve targeting delivery and inhibition of tumor growth and angiogenesis simultaneously. The cytotoxicity, inhibiting angiogenesis, and internalization of various liposomes by cells were assessed *in vitro* to confirm the influence of the peptide modification. The accumulations of A7RC-LIPs in various xenografts in mice were tracked to further identify the function of the peptide on the liposomes surface. The results confirmed that A7RC peptide could enhance the uptake of vesicles by MDA-MB-231 cells, leading to stronger cytotoxicity *in vitro* and higher accumulation of vesicles in MDA-MB-231 xenografts *in vivo*. In addition, A7RC peptide enhanced the inhibitory effects of LIPs on the HUVECs tubular formation on Matrigel. The A7RC-LIPs may be promising drug carriers for anticancer therapy.

Key words: Liposomes; paclitaxel; A7RC; Neuropilin-1; breast cancer.

Background

Paclitaxel is a natural plant product extracted from bark of western taxus brevifolia[1]. It's a potent antimitotic chemotherapeutic drug used against various cancers[2-4]. However, chemotherapy with paclitaxel has been limited due to the severe hypersensitivity reactions and other adverse side effects that include neurotoxicity and nephrotoxicity caused by cremophor EL[5, 6]. To overcome the challenges of paclitaxel solubility and toxicity, many efforts have been made to develop improved drug delivery systems such as liposomes and micelles [6-13]. The innate physico-chemical properties of nanoscale carriers impact the clinic application of the formulations[14]. Liposomal formulations represent one of the advanced and promising delivery systems for chemotherapeutics [15-21]. Studies have demonstrated that encapsulation of paclitaxel into liposomes (Lipusu ®) improved therapeutic efficacies and reduced toxic effects [22-24]. In addition, the studies have confirmed that the isolation of docetaxel and tamoxifen by polymers inhibit the antagonistic effects[25]. Recently, researchers have designed active targeted liposomes to direct the antitumor drugs to the tumor cells or tumor blood vessels by attaching specific ligands on the surface of liposomes, including antibody molecules or their fragments, naturally or synthetic ligands such as peptides, glycoproteins or carbohydrates [26]. Various studies have revealed that actively targeted liposomes could increase the specificity of loaded drugs to targeting cells and reduce the undesirable side effects on healthy organs comparing to non-targeted liposomes [27, 28].

Biodiveristy of tumor requires specific strategy for breast cancer cells.

Neuropilin 1 (NRP-1), the single-pass transmembrane glycoproteins, was first discovered as regulator in neural development[29]. Subsequently, as VEGF co-receptor, NRP-1 has been identified as a non-tyrosine kinase receptor of vascular endothelial growth factor-165 (VEGF165). The co-expression of NRP-1 and VEGFR-2 can significantly increase VEGF165 binding to VEGFR-2, thereby enhancing VEGF165-mediated signaling networks and playing the important role in blood vessel formation and survival [30-32]. Additionally, NRP-1 has been shown to highly expressed in a variety of human tumors, including breast, lung, ovary, urologic neoplasms, and gastroenteric tumor[33, 34]. Recent evidences have reported that overexpression of NRP-1 can enhance tumor-mediated angiogenesis, tumor growth, invasion, and metastasis, which has spurred a strong interest in NRP-1 as a potential anti-tumor target [33, 35].

Small peptides which selectively binding tumor cells or tumor blood vessels surface markers have emerged as one of the most valuable non-immunogenic approaches to target cells [36, 37]. A targeting peptide binding to NRP-1 receptor may be a candidate that can be used to enhance the therapeutic efficacy of paclitaxel liposomes. The low molecular weight heptapeptide ATWLPPR(A7R) identified by screening a mutated phage library can selectively bind NRP-1 receptor, based on previous studies on tumor angiogenesis and metastasis [38, 39].

In this study, we first prepared paclitaxel liposomes conjugated with the A7RC sequence with thiol group. Then, high and low NRP-1 expressing breast cancer cell lines and human umbilical vein endothelial cells (HUVECs) were used to further

evaluate the cytotoxicity and antiangiogenic effects of different paclitaxel formulations *in vitro*. Finally, the cellular uptake and tumor tissue distribution of different liposomal paclitaxel formulations *in vitro* and *in vivo* were determined. The results showed that conjugating the targeting peptide A7RC to paclitaxel liposomes significantly enhanced the targeting efficiency in high NRP-1 expressing MDA-MB-231 cells. Moreover, after A7RC peptide modification, the antiangiogenic effect of paclitaxel liposomes was significantly improved on medium NRP-1 expressing HUVECs. All the results suggested that A7RC peptide modified liposomal paclitaxel could be a promising strategy for enhancing the antitumor and antiangiogenic effects in the individualized breast cancer chemotherapy.

Methods

Materials

Cholesterol (CHO) and Egg phosphatidylcholine (EPC) were obtained from Bio Life Science & Technology Co., Ltd. (Shanghai, China). Distearoylphosphosphatidyl-ethanolamine (DSPE-PEG2000) was purchased from NOF Corporation (Tokyo, Japan). Various tracking probes including rhodamine B (Rho), 1,1'-dioctadecyl-3,3,3',3'-tetramethylindotricarbocyanine iodide (DiR), 3,3-dioctadecyloxacarbocyanine perchlorate (DiO), and Hoechst 33258 were obtained from Beijing Fanbo Science & Technology, Co. Ltd (Beijing, China). A7R-cysteine peptides (ATWLPPRC) were synthesized by Shanghai Qiangyao Co. Ltd. Paclitaxel was purchased from Beijing Unions Pharma Company (Beijing, China).

Conjugation of A7RC peptide with DSPE-PEG maleimide

The connection of thiol group of A7RC peptide with 1,2-distearoyl-sn-glycero-3-phosphoethanolamine-N-[maleimide(polyethylene glycol)-2000] (DSPE- PEG(2000) Maleimide) was achieved according to previous method [40]. Briefly, A7RC peptides and 1,2-distearoyl-sn-glycero-3-phosphoethanolamine-N-[maleimide(polyethylene glycol)-2000] (DSPE- PEG(2000) Maleimide) (1/1 as molar ratio) were added into HEPES solution and reacted at 4 °C for 12 h. The coupling efficiency of resultant conjugates was determined with high performance liquid chromatography (HPLC) system with a UV detector (Agilent Technologies Inc, Cotati, CA). An ODS column (Diamonds, 250×4.6 mm, 5 μm) was used for analysis and the column temperature was 30°C. All samples were analyzed in triplicate (A=29145196.58C+57089.94434, r^2=0.998).

Preparation of liposomes

LIPs and A7RC-LIPs were prepared according to the method previous reported [40-42]. Briefly, cholesterol, egg phosphatidylcholine, distearoylphosphphosphatidylethanolamine (PEG2000-DSPE) (43/52/4.5 as molar ratio), and paclitaxel or dyes (rhodamine (Rho), DiR) (drug: lipid= 1:10; W/W) were dissolved in the mixture of anhydrous alcohol and chloroform and then removed the organic solvent with a rotary evaporator. The resultant film was hydrated and further dispersed using a probe sonicator at 100w for 50 s, and sequentially extruded through

220- and 100-nm polycarbonate membranes for 3 times. After extrusion, the suspensions were further dialyzed against the isotonic PBS to obtain the LIPs. The A7RC-LIPs were acquired by post-insertion process according to the previous methods [40].

Characterization of liposomes

Size and zeta potential

The surface charge and size distribution of liposomes including the LIPs and A7RC-LIPs were determined using a Malvern Zetasizer Nano ZS 90 instrument (Malvern Instruments, Ltd., UK). The morphology and size of both liposomes were also observed using transmission electron microscope (TEM, Tecnai G2 F20, STEM; FEI, Hillsboro) and atomic force microscope (AFM, Nanoscope III Digital Instruments/Veeco, Santa Barbara). As for AFM, the samples were dropped onto a mica surface, and the solution was evaporated at room temperature over 24 hours[43].

Encapsulation efficiency and drug release behavior

The paclitaxel in the LIPs and A7RC-LIPs were analyzed with same HPLC equipment and analyzing column ($A=36865C+21403$, $r^2=0.9994$) with peptide. However, the detection wavelength was set to 227 nm and mobile phase was a mixture of acetonitrile and water (60/40, v/v). Encapsulated efficiencies of paclitaxel in both liposomes were evaluated. The release kinetics of drug from liposomes was recorded for 24 h by HPLC according to previous method [44].

Cell culture

Human breast cancer cell lines MDA-MB-231 and MCF-7 were grown on culture flasks in monolayers and maintained in Dulbecco's modified Eagle's medium (DMEM; Invitrogen, Carlsbad, CA) supplemented with 10 % fetal bovine serum (FBS; Hyclone, Logan, UT), penicillin (100 units/ml), and streptomycin (100 units/ml) at 37 °C in a humid atmosphere of 5 % CO_2 and 95 % air. HUVECs were grown in F-12K Medium (Invitrogen, Carlsbad, CA) added 0.03 mg/ml endothelial cell growth supplement (ECGS; Millipore, Billerica, MA) and supplemented with 10 % fetal bovine serum (FBS; Hyclone, Logan, UT) at 37 °C in a humidified 5 % CO_2 incubator. All cells were free of bacteria, viruses, and mycoplasma.

Western blot analysis

Western blot analysis was performed as described previously [45]. Briefly, cells were harvested and lysed in the lysis buffer. The protein concentration was determined by the BSA protein assay kit quantification (Bio-Rad Laboratories, Hercules, CA). Expression of NRP-1 was determined with horseradish peroxidase-conjugated anti-goat immunoglobulin G (1:2000; Santa Cruz Biotechnology, Santa Cruz, CA) and revealed by enhanced chemiluminescence reagent (Amersham Pharmacia Biotech, Piscataway, NJ) according to the manufacturer's suggested protocols. An anti-α-tubulin mouse monoclonal antibody (1:1000; Santa Cruz Biotechnology) was used to confirm equal loading. Densitometry

analysis processed using ImageJ software.

In vitro cytotoxicity assays

Cytotoxicity tests were evaluated by 3-(4,5-dimethylthiazol-2-yl)-2,5-diphenyl-tetrazolium bromide (MTT) (Sigma, St. Louis, MO, USA) assay. Cells were resuspended in 96-well microtiter plates at appropriate densities. After 24 h, cells were adherent to the plate and the culture medium was replaced with 200 μl different concentrations of free paclitaxel, LIPs, and A7RC-LIPs. The medium was removed after 68 h later and replaced with 200 μl of MTT at the concentration of 1 mg/ml for additional 4 h. The formazan crystals were dissolved in 150 μl of dimethylsulfoxide (DMSO, Sigma). Absorbance was determined at 570 nm in a multi-detection microplate reader (BIO-RAD). The percentage of viable cells was compared to untreated cells. The concentrations required to inhibit growth by 50 % (IC50) were calculated from survival curves using the Bliss method [46]. All treatments were performed in quadruplicate and experiments were repeated three times.

In vitro endothelial cell tube formation

Fifty microliters of Unpolymerized growth factor-reduced Matrigel (BD Biosciences, Bedford, MA) was applied to each well of a 96-well plate and allowed to polymerize for 30 min at 37 °C. HUVECs (3×10^3 cells/well) were suspended in 100 μl culture medium containing 1 % FBS and 10 ng/ml bFGF (PeproTech, Rocky Hill, NJ), and seeded onto the top of Matrigel layer, then incubated at 37 °C. After 6h, HUVECs

were formed capillary-like networks. Adherent cells received A7RC, free paclitaxel, LIPs, and A7RC-LIPs at the indicated concentrations respectively. After 24 h treatment, *in vitro* angiogenesis was observed under the inverted phase-contrast microscope (Olympus IX71). For quantitative analysis, images were photographed from five random microscopic fields per well, and measured the number of branch points and the total length of tubes using ImageJ software. Experiments were performed in duplicate for each condition and repeated three times.

Cellular uptake

Flow cytometry analysis

The cellular uptakes of Rho-labeled LIPs by endothelial and cancerous cells were measured using a FACS (Becton Dickinson FACS Aria I, Mountain View, CA, USA)[47]. The cells were cultured for 24 h on the six-well culture plate and grown to confluence prior to the measurement. Free Rho, Rho-labeled LIPs, Rho-labeled A7RC-LIP were respectively added to the different wells of the plate, and then the cells were maintained at 37 °C with 5 % CO_2. The dye-free culture medium was used as a blank control. After 4h incubation, cells were collected to test the fluorescence signal by the flow cytometer. Ten thousand events were calculated, and the data were processed using FlowJo 7.6 software.

Time-Lapse live cell imaging

Uptakes of liposomes by endothelial and cancerous cells were monitored using a

Delta Vision microscope system (Applied Precision, Issaquah, WA, USA). The HUVECs and the breast cancer cell lines MDA-MB-231 and MCF-7 were evenly seeded onto plates (Applied Precision) and maintained for 24 h at 37 °C in the presence of 5 % CO_2. Before imaging, cell nuclei were stained with Hoechst 33258 (5 µg/mL) while membrane with DiO (5 µg/mL), then followed with triplicate rinse of PBS. Thereafter, Rho-labeled A7RC-LIPs were added and live-cell imaging was started right away. Fluorescence images were captured for 30 min and data were processed using Delta Vision SoftWoRx software.

In vivo imaging

Animals

Female BALB/c nude mice weighing 16–20 g were provided by Peking University Health Science Center (Beijing, China) and raised at Harbin Medical University (Daqing) in sterile microisolator cages at 20 ± 2 °C and 45 ± 5 % humidity. All animal handling and experimental procedures were performed in accordance with the *Guide for the Care and Use of Laboratory Animals* published by the US National Institutes of Health (NIH Publication No. 85-23, revised 1996). All the animals were monitored daily by animal care staff and were under humane treatment during the experiments.

Inoculation

Cancerous cells were cultured in proper flasks at 37 °C in a humidified atmosphere (90 % humidity) with 5 % CO2. Before inoculation, the MDA-MB-231 or MCF-7 cells were trypsinized and rinsed with PBS to remove the cultural media. The resultant cells were resuspended in serum-free DMEM. 200 μl of cell suspensions (approximately 0.5×10^7 cells) was subcutaneously inoculated into the armpits of mice.

In vivo imaging

When tumor volumes reached approximately 400–500 mm^3 (calculated as length × width^2/2), the mice were injected with 0.2 mL of the DiR-labeled LIPs or DiR-labeled A7RC-LIPs via the tail vein. The distribution of fluorescence intensity in tissues was imaged using a Kodak multimodel imaging system (Carestream Health, Inc., Rochester, New York, USA). Four hours after injection, the images of signal distribution in mice were obtained. After image of whole body, mice were anaesthetized and tumor tissues were immediately removed, rinsed with PBS, and the fluorescent images of the tumor tissues were obtained. The signal strength in whole body and xenografts were determined at excitation and emission wavelengths of 747 and 774 nm, respectively.

Statistical analysis

All of the data were expressed as the mean ± standard deviation (S.D.). The statistical analyses were determined using one-way analysis of variance (ANOVA)

between groups. *P<0.05* was considered to indicate a statistically significant difference; *P<0.001* was considered to indicate an extremely significant difference.

Results

Characterization of the liposomes

The average particle sizes of all liposomes were approximately 100 nm (Fig. 1A-C). Particulate size of A7RC-LIPs was slightly bigger than that of LIPs. The morphology of vesicles by TEM (Fig. 1A) and AFM (Fig. 1B) clearly showed that A7RC-LIPs were spherical in shape and had sizes around 100 nm. The charge values of vesicles surface were about -15 mV (Fig. 1D). The conjugating efficiency of A7RC in A7RC-LIPs was > 90 %. The encapsulated efficiency of drug and fluorescent dyes (DiR or Rho) from liposomes was 96.4±2.1%, 82.3±1.8% or 46.7±2.3%, and the drug and fluorescent dyes (DiR or Rho) release rate from liposomes during 24 h was 22.5±1.1%, 25.8%±1.3 or 64.3±2.5%, respectively.

NRP-1 expression level

NRP-1 is a key receptor expressed by endothelial and some tumor cells and plays an important role in tumor angiogenesis and progression [48]. According to previous studies on NRP-1 of breast cancer [38, 49], we selected cell lines expressing high (MDA-MB-231) and low (MCF-7) levels of NRP-1 as cultured breast cancer cell lines and HUVECs as cultured vascular endothelial cell line. To examine the expressing levels of NRP-1, western blotting analysis was conducted on HUVECs,

MDA-MB-231 and MCF-7 cell lines. The results showed that MDA-MB-231 cells expressed higher level of NRP-1 protein as compared with MCF7 cells, and HUVECs expressed medium level of NRP-1 protein when compared with two breast cancer cell lines (Fig. 2). Western blotting densitometry analysis indicated that there were a 1.8-fold increase in HUVECs and a 5.4-fold increase in MDA-MB-231 cells compared to MCF-7 cells, which suggested that NRP-1 expressing levels are different among different breast cancer cells and vascular endothelial cells.

Enhanced the cytotoxicity on high NRP-1 expressing cell

Since overexpression of NRP-1 was observed in MDA-MB-231 cells and HUVECs, we then analyzed whether high NRP-1 expressing cell lines were sensitive to A7RC-LIPs. We first explored the cytotoxic effect of A7RC peptide alone in MDA-MB-231 cell line, MCF-7 cell line, and HUVECs. As shown by the dose-response curves in Fig. 3A, treatment with A7RC peptide alone only exhibited a minor inhibitory effect, and the survival rate of three cell lines was still more than 75% even at concentration of 100 μM. The results indicated that A7RC alone has little cytotoxicity and cannot inhibit proliferation in those low, medium, and high expressing NRP-1 cell lines. We next evaluated the cytotoxicity effects of three paclitaxel formulations on above mentioned cells. The dose-response curves and the mean IC50 values are shown in Fig. 3B-D. In MDA-MB-231 cell line, which manifested high expression of NRP-1, the dose-response curve of A7RC-LIPs was clearly shifted to left when compared with free paclitaxel or LIPs (Fig. 3B). The IC50

value of A7RC-LIPs exhibited a greater than 4-fold reduction compared to LIPs

(0.134±0.031 μM versus 0.541±0.076 μM) and 6-fold reduction compared to free

paclitaxel (0.134±0.031 μM versus 0.806±0.132 μM). In HUVECs, which showed

medium expression of NRP-1, the dose-response curve of A7RC-LIPs was slightly

shifted to left when compared with free paclitaxel or LIPs (Fig. 3C). And the IC50

value of A7RC-LIPs exhibited 1.5-fold reduction compared to LIPs (8.37±1.21 nM

versus 12.82±2.14 nM) and over 2-fold reduction compared to free paclitaxel

(8.37±1.21 nM versus 16.76±2.66 nM). However, in MCF-7 cell line, which showed

low expression of NRP-1, the dose-response curve of A7RC-LIPs was not shifted

when compared to LIPs, and the IC50 value of A7RC-LIPs was almost as same as

LIPs. The IC50 values of A7RC-LIPs, LIPs and free paclitaxel were 1.104±0.292 μM,

1.089±0.311 μM, and 1.458±0.262 μM, respectively (Fig. 3D). Our data supported

that A7RC-LIPs could significantly enhance the cytotoxicity effects on high NRP-1

expressing breast cancer cells and medium NRP-1 expressing vascular endothelial

cells, but not on low NRP-1 expressing cells.

Enhanced the inhibitory effect on formation of tubule-like structures

The endothelial cell tube formation assay was used to assess the antiangiogenesis

effects of A7RC and three paclitaxel formulations *in vitro*. HUVECs plated on

Matrigel with bFGF formed a typical tube-like structure, which reflected the

angiogenic capacity (Fig. 4A). The results showed that A7RC had slightly inhibitory

effect on vessel formation even at concentration of 100μM (Fig. 4B). It suggested that

A7RC alone cannot significantly inhibit bFGF-induced tube-like formation. Based on the dose-dependent inhibition curve of HUVECs, we selected similar concentration of different paclitaxel formulations to perform tube formation assay. The results showed that addition of 10nM A7RC-LIPs significantly inhibited tube formation of HUVECs in the vicinity (Fig. 4E), and addition of 10 nM LIPs showed relatively medium inhibition (Fig. 4D), whereas addition of 10 nM free paclitaxel showed relatively weak inhibition (Fig. 4C). Quantitative analysis further indicated that the number of branching junctions and length of tube-like structures were decreased significantly by A7RC-LIPs ($P<0.001$), and more mildly but significantly reduced by LIPs ($P<0.01$). Free paclitaxel group also manifested the weak inhibitory effect on vessel formation when compared with control ($P<0.05$). However, A7RC group had not showed significantly inhibitory effect on vessel formation by quantitative analysis (Fig. 4F and G). Those results suggested that A7RC-LIPs have a higher inhibitory effect than LIPs on formation of tube-like structures of HUVECs *in vitro*.

Intracellular uptake of liposomal paclitaxel in different formulations

Flow cytometry assay was used to evaluate the cellular uptake of A7RC-LIPs and LIPs in each cell line after incubated with Free Rho, Rho-labeled LIPs, and Rho-labeled A7RC-LIPs for 4 hours. The data confirmed that the intracellular uptake of LIPs was higher than that of free Rho in all the three cell lines (Fig.5A-C). Additionally, the uptakes of A7RC-LIPs were greatly increased in MDA-MB-231 cells (Fig.5B) and HUVECs (Fig. 5C) when compared to LIPs. However, there was

not any significant internalized difference between MCF-7 cells incubated with A7RC-LIPs or with LIPs (Fig.5A). Those results confirmed that LIPs after A7RC modification were much more internalized by high NRP-1 expressing MDA-MB-231 cells and medium NRP-1 expressing HUVECs than low NRP-1 expressing MCF-7 cells.

Intracellular distribution of A7RC-LIPs

Time-lapse live cell imaging assay was performed to investigate the intracellular distribution of Rho-labeled A7RC-LIPs in different levels of NRP-1 expressing cell lines. As shown in Fig. 6A, during 30 min incubation with A7RC-LIPs, red fluorescence signal were intensively distributed in cytoplasm in MDA-MB-231 cells and HUVECs, which expressing high and medium level of NRP-1. However, there was little uptake of A7RC-LIPs by MCF-7 cells, which expressing low level of NRP-1. At the end of 30 min, the relative fluorescence intensity increased to 200 in MDA-MB-231 cells, 70 in HUVECs, and 5 in MCF-7 cells, respectively (Fig. 6B). Those results demonstrated that A7RC-LIPs could be much more internalized by high NRP-1 expressing breast cancer cells and medium NRP-1 expressing HUVECs. Therefore, A7RC-LIPs may have a stronger antitumor and antiangiogenesis effect on high NRP-1 expressing cells than low NRP-1 expressing cells.

Tissue distribution of liposomal paclitaxel formulations

After known the uptake and distribution of LIPs and A7RC-LIPs *in vitro*, we

next assessed the tissue-distribution profiles of the two liposomal formulations in nude mice. DiR-labeled LIPs or DiR-labeled A7RC-LIPs were intravenously injected into nude mice bearing MCF-7 and MDA-MB-231 tumor respectively. As shown in Fig. 7A and B, 4 hours after administration, the fluorescence intensity in mice injected with A7RC-LIPs was stronger than that in animals injected with LIPs in MDA-MB-231 xenograft models. Analysis demonstrated that the relative fluorescence intensity in mice injected with A7RC-LIPs was significantly different from that in mice injected with LIPs ($P<0.05$). However, the fluorescence intensity in mice injected with A7RC-LIPs was only slightly changed in MCF-7 xenograft models in comparison with that in animals injected with LIPs. There is no significant difference between A7RC-LIPs injected animals and LIPs injected animals ($P>0.05$). Those results supported that A7RC-LIPs enhanced the dye accumulation in local tumor tissue where NRP-1 was overexpressed.

To further confirm the observed fluorescence signal truly came from xenografts themselves, we excised the tumor tissue and examined the fluorescence intensity. As shown in Fig. 7C and D, A7RC-LIPs more strongly accumulated in MDA-MB-231 xenografts than LIPs after administration of drugs ($P<0.05$). However, the fluorescence intensity of tumors was not significant increased with administration of A7RC-LIPs in MCF-7 xenografts as compared with LIPs ($P>0.05$). Overall, the *ex vivo* tissue distribution experiments demonstrated that LIPs after A7RC modification selectively enhanced the targeting accumulation in NRP-1 overexpressing breast cancer cells.

Discussion

People have constructed the 3D cancer model to understand the relevance between the *in vivo* data and the in *vitro* data after the therapy of the nanomedicine [50]. The nanocarriers may induce endothelial cell leakage by the innate properties such as titanium dioxide nanomaterials but cytotoxic effects of drugs in the tumor tissue, inhibiting the angiogensis in the xenograt [51]. The researchers have endeavored to enhance the cytotoxic effects of chemotherapeutics, especially for the negative breast cancer cells[52]. Some markers on the breast cancer cells can be used to design the nanocarriers, enhancing the sensitivity of cancer cells to the chemotherpeutics.

In this study, we created a targeted paclitaxel liposomes conjugated with small peptide A7RC which contains specific sequence to NRP-1 receptor. We further studied the biological effects on cells and cellular uptake and distribution of A7RC-LIPs in breast cancer cell lines and HUVECs.

The results revealed that the encapsulation efficiencies of paclitaxel in LIPs and A7RC-LIPs were 97.4 ± 2.3 % and 96.4 ± 2.1%, respectively. Therefore, there was no significantly influence on the loading efficiency due to modification process. The results from TEM and AFM showed that the mean particle sizes of the two paclitaxel liposomes were similar (approximately 100 nm), which suggested that conjugation of the peptide A7RC did not influence the size of liposomes too much. The size data from TEM and AFM was slightly smaller than dynamic light scattering. The size of liposomes under 100 nm are more suitable for penetrating the physical barrier and

entering into targeted cells after intravenous administration[53]. Small size modified liposomes can further improve target localization by prolonging the circulation time and/or binding to specific receptors[54].

More and more data have confirmed that NRP-1 is over-expressed in a wide variety of human tumor types [55, 56]. Moreover, overexpression of NRP-1 can promote tumor growth and invasion, leading to poor prognosis [57, 58]. Recent study has confirmed that A7R peptide can regulate the $VEGF_{165}$ interactions with NRP-1 and plays potential roles in decreasing tumor angiogenesis and growth [38]. Interestingly, we did not observe the direct cytotoxic effect of A7RC peptide in all the three cell lines even at concentration of 100 μM, which was not achievable in the process of A7RC-LIPs. Our data indicated that A7RC peptide did not suppress the proliferation of breast cancer cells and HUVECs at relatively high concentration. However, we found that the cytotoxicity of A7RC-LIPs was more increased than that of LIPs in high NRP-1 expressing MDA-MB-231 cells and slightly increased in medium NRP-1 expressing HUVECs, whereas it was not enhanced in low NRP-1 expressing breast cancer MCF-7 cells. Our results indicated that A7RC-LIPs significantly improved the proliferation inhibitory effects compared with conventional liposomal formulations on high NRP-1 expressing breast cancer cells. The explanation could account that A7RC more effectively provided specific target binding and formed ligand-mediated internalization of liposomes in overexpressing NRP-1 breast cancer cells, which was in general agreement with Zhou and his colleagues' study on A549 human lung adenocarcinoma cell line and HUVECs [28].

In addition to the improved inhibitory effects on proliferation of MDA-MB-231 cells and HUVECs, our *in vitro* findings from tube formation assay suggested that A7RC-LIPs also increased the antiangiogenic effects on medium NRP-1 expressing HUVECs compared with LIPs. We did not observe the inhibiting effect of A7RC on bFGF-induced formation of vessel-like structures *in vitro* at a high concentration. However, A7RC-LIPs showed much more inhibiting effect than LIPs on the vessel formation *in vitro*. Those data indicate that A7RC promoted the internalization of LIPs to HUVECs. Therefore, A7RC-LIPs may exert better antiangiogenic effects on NRP-1 overexpressing vessel endothelial cells.

In order to further investigate the uptake and distribution of A7RC-LIPs in different NRP-1 expressing cells, we performed flow cytometry and time-lapse live cell imaging experiments. The fluorescence intensity in MDA-MB-231 cells and HUVECs incubated with A7RC-LIPs was higher than that incubated with LIPs. After incubated with A7RC-LIPs, however, lower fluorescence intensity in MCF-7 cells than in MDA-MB-231 cells and HUVECs is due to the lower expression of NRP-1 in MCF-7 cells. Those results demonstrated that the amount of paclitaxel liposomes uptake and distribution is dependent on the level of NRP-1 expression on the cell surface. Our data also suggested that A7RC significantly improved the targeting efficacy of paclitaxel liposomes in high NRP-1 expressing cells, which may contribute to receptor mediated cellular endocytosis.

Meanwhile, the results from *in vivo* imaging study showed that the mean fluorescence intensity in tumor local tissues for DiR-labeled A7RC-LIPs was stronger

than that for LIPs in high NRP-1 expressing tumor xenografts. Those results proved

that A7RC-LIPs were able to enhance the uptake and accumulation in high NRP-1

expressing tumor xenografts rather than in low NRP-1 expressing tumor xenografts.

High tumor tissue local accumulation may provide more opportunity to enhance the

antitumor effects and reduce toxicity to normal tissues. Future work is required to

confirm the inhibitory effect on tumor growth *in vivo*.

Acknowledgements

Reference

1. E. K. Rowinsky and R. C. Donehower, *N Engl J Med*, 1995, **332**, 1004-1014.

2. N. I. Marupudi, J. E. Han, K. W. Li, V. M. Renard, B. M. Tyler and H. Brem, *Expert Opin Drug Saf*, 2007, **6**, 609-621.

3. K. E. Gascoigne and S. S. Taylor, *J Cell Sci*, 2009, **122**, 2579-2585.

4. M. Tahara, H. Minami, Y. Hasegawa, K. Tomita, A. Watanabe, K. Nibu, M. Fujii, Y. Onozawa, Y. Kurono and D. Sagae, *Cancer chemotherapy and pharmacology*, 2011, **68**, 769-776.

5. R. B. Weiss, R. C. Donehower, P. H. Wiernik, T. Ohnuma, R. J. Gralla, D. L. Trump, J. R. Baker, Jr., D. A. Van Echo, D. D. Von Hoff and B. Leyland-Jones, *J Clin Oncol*, 1990, **8**, 1263-1268.

6. A. Safavy, *Curr Drug Deliv*, 2008, **5**, 42-54.

7. R. V. Kutty, S. L. Chia, M. I. Setyawati, M. S. Muthu, S. S. Feng and D. T. Leong, *Biomaterials*, 2015, **63**, 58-69.

8. S. Singh and A. K. Dash, *Crit Rev Ther Drug Carrier Syst*, 2009, **26**, 333-372.

9. H.-s. Peng, X.-j. Liu, G.-x. Lv, B. Sun, Q.-f. Kong, D.-x. Zhai, Q. Wang, W. Zhao, G.-y. Wang and D.-d. Wang, *International journal of pharmaceutics*, 2008, **352**, 29-35.

10. Z.-f. Hao, Y.-x. Cui, M.-h. Li, D. Du, M.-f. Liu, H.-q. Tao, S. Li, F.-y. Cao, Y.-l. Chen and X.-h. Lei, *European Journal of Pharmaceutics and Biopharmaceutics*, 2013, **84**, 505-516.

11. H.-q. Tao, Q. Meng, M.-h. Li, H. Yu, M.-f. Liu, D. Du, S.-l. Sun, H.-c. Yang, Y.-m. Wang and W. Ye, *Naunyn-Schmiedeberg's archives of pharmacology*, 2013, **386**, 61-70.

12. M. Li, H. Deng, H. Peng and Q. Wang, *Journal of nanoscience and nanotechnology*, 2014, **14**, 415-432.

13. Y. Yang, S. Wang, Y. Wang, X. Wang, Q. Wang and M. Chen, *Biotechnology advances*, 2014.

14. M. I. S. Chor Yong Tay, Jianping Xie, Wolfgang J. Parak, and David Tai Leong., *Adv. Funct. Mater.*, 2014, **24**, 5936-5955.

15. R. D. Hofheinz, S. U. Gnad-Vogt, U. Beyer and A. Hochhaus, *Anticancer Drugs*, 2005, **16**, 691-707.

16. S. Mallick and J. S. Choi, *J Nanosci Nanotechnol*, 2014, **14**, 755-765.

17. M. Shao, S.-l. Sun, M.-h. Li, B.-x. Li, H. Yu, Z.-y. Shen, Y.-c. Ren, Z.-f. Hao, N.-d. Chang and H.-s. Peng, *Journal of liposome research*, 2012, **22**, 168-176.

18. M. Li, H. Yu, T. Wang, N. Chang, J. Zhang, D. Du, M. Liu, S. Sun, R. Wang, H. Tao, Z. Shen, Q. Wang and H. Peng, *Journal of Materials Chemistry B*, 2014, **2**, 1619-1625.

19. F. Jia, X. Liu, L. Li, S. Mallapragada, B. Narasimhan and Q. Wang, *Journal of Controlled Release*, 2013, **172**, 1020-1034.

20. M. Liu, M. Li, G. Wang, X. Liu, D. Liu, H. Peng and Q. Wang, *Journal of Biomedical Nanotechnology*, 2014, **10**, 2038-2062.

21. R. Bi, W. Shao, Q. Wang and N. Zhang, *Journal of drug targeting*, 2008, **16**, 639-648.

22. R. M. Straubinger and S. V. Balasubramanian, *Methods Enzymol*, 2005, **391**, 97-117.

23. Z. Zhang, L. Mei and S. S. Feng, *Expert Opin Drug Deliv*, 2013, **10**, 325-340.

24. L. Ye, J. He, Z. Hu, Q. Dong, H. Wang, F. Fu and J. Tian, *Food and Chemical Toxicology*, 2013, **52**, 200-206.

25. G. R. Tan, S. S. Feng and D. T. Leong, *Biomaterials*, 2014, **35**, 3044-3051.

26. S. Koudelka and J. Turanek, *J Control Release*, 2012, **163**, 322-334.

27. A. Catania, E. Barrajon-Catalan, S. Nicolosi, F. Cicirata and V. Micol, *Breast Cancer Res Treat*, 2013, **141**, 55-65.

28. S. Meng, B. Su, W. Li, Y. Ding, L. Tang, W. Zhou, Y. Song, H. Li and C. Zhou, *Nanotechnology*, 2010, **21**, 415103.

29. A. L. Kolodkin, D. V. Levengood, E. G. Rowe, Y. T. Tai, R. J. Giger and D. D. Ginty, *Cell*, 1997, **90**, 753-762.

30. S. Soker, S. Takashima, H. Q. Miao, G. Neufeld and M. Klagsbrun, *Cell*, 1998, **92**, 735-745.

31. E. A. Jones, L. Yuan, C. Breant, R. J. Watts and A. Eichmann, *Development*, 2008, **135**, 2479-2488.

32. C. A. Staton, I. Kumar, M. W. Reed and N. J. Brown, *J Pathol*, 2007, **212**, 237-248.

33. A. Bagri, M. Tessier-Lavigne and R. J. Watts, *Clin Cancer Res*, 2009, **15**, 1860-1864.

34. D. R. Bielenberg and M. Klagsbrun, *Cancer Metastasis Rev*, 2007, **26**, 421-431.

35. Q. Pan, Y. Chanthery, W. C. Liang, S. Stawicki, J. Mak, N. Rathore, R. K. Tong, J. Kowalski, S. F. Yee, G. Pacheco, S. Ross, Z. Cheng, J. Le Couter, G. Plowman, F. Peale, A. W. Koch, Y. Wu, A. Bagri, M. Tessier-Lavigne and R. J. Watts, *Cancer Cell*, 2007, **11**, 53-67.

36. H. Slimani, E. Guenin, D. Briane, R. Coudert, N. Charnaux, A. Starzec, R. Vassy, M. Lecouvey, Y. G. Perret and A. Cao, *J Drug Target*, 2006, **14**, 694-706.

37. K. N. Sugahara, T. Teesalu, P. P. Karmali, V. R. Kotamraju, L. Agemy, O. M. Girard, D. Hanahan, R. F. Mattrey and E. Ruoslahti, *Cancer Cell*, 2009, **16**, 510-520.

38. A. Starzec, R. Vassy, A. Martin, M. Lecouvey, M. Di Benedetto, M. Crepin and G. Y. Perret, *Life Sci*, 2006, **79**, 2370-2381.

39. R. Binetruy-Tournaire, C. Demangel, B. Malavaud, R. Vassy, S. Rouyre, M. Kraemer, J. Plouet, C. Derbin, G. Perret and J. C. Mazie, *EMBO J*, 2000, **19**, 1525-1533.

40. M. Liu, M. Li, S. Sun, B. Li, D. Du, J. Sun, F. Cao, H. Li, F. Jia, T. Wang, N. Chang, H. Yu, Q. Wang and H. Peng, *Biomaterials*, 2014, **35**, 3697-3707.

41. H. Peng, D. Du and J. Zhang, *Therapeutic delivery*, 2013, **4**, 1475-1477.

42. D. Du, N. Chang, S. Sun, M. Li, H. Yu, M. Liu, X. Liu, G. Wang, H. Li, X. Liu, Q. Wang and H. Peng, *Journal of Controlled Release*, 2014, **182**, 99-110.

43. C. M. Paleos, Z. Sideratou and D. Tsiourvas, *The Journal of Physical Chemistry*, 1996, **100**, 13898-13900.

44. H.-J. Yao, R.-J. Ju, X.-X. Wang, Y. Zhang, R.-J. Li, Y. Yu, L. Zhang and W.-L. Lu, *Biomaterials*, 2011, **32**, 3285-3302.

45. L. B. Song, M. S. Zeng, W. T. Liao, L. Zhang, H. Y. Mo, W. L. Liu, J. Y. Shao, Q. L. Wu, M. Z. Li, Y. F. Xia, L. W. Fu, W. L. Huang, G. P. Dimri, V. Band and Y. X. Zeng, *Cancer Res*, 2006, **66**, 6225-6232.

46. Z. Shi, Y. J. Liang, Z. S. Chen, X. W. Wang, X. H. Wang, Y. Ding, L. M. Chen, X. P. Yang and L. W. Fu, *Cancer Biol Ther*, 2006, **5**, 39-47.

47. A. Beduneau, F. Hindre, A. Clavreul, J. C. Leroux, P. Saulnier and J. P. Benoit, *Journal of controlled release : official journal of the Controlled Release Society*, 2008, **126**, 44-49.

48. A. M. Jubb, L. A. Strickland, S. D. Liu, J. Mak, M. Schmidt and H. Koeppen, *J Pathol*, 2012, **226**, 50-60.

49. A. Kumar, H. Ma, X. Zhang, K. Huang, S. Jin, J. Liu, T. Wei, W. Cao, G. Zou and X. J. Liang, *Biomaterials*, 2012, **33**, 1180-1189.

50. D. T. Leong and K. W. Ng, *Advanced drug delivery reviews*, 2014, **79-80**, 95-106.

51. M. I. Setyawati, C. Y. Tay, S. L. Chia, S. L. Goh, W. Fang, M. J. Neo, H. C. Chong, S. M. Tan, S. C. Loo, K. W. Ng, J. P. Xie, C. N. Ong, N. S. Tan and D. T. Leong, *Nature communications*, 2013, **4**,

   1673.

52. C. Y. T. Rajaletchumy Veloo Kutty, Chen Siew Lim, Si-Shen Feng, and David Tai Leong, *Nano Research*, 2015, DOI: 10.1007/s12274-015-0760-8.

53. N. Oku, *Adv Drug Deliv Rev*, 1999, **40**, 63-73.

54. J. M. van den Hoven, S. R. Van Tomme, J. M. Metselaar, B. Nuijen, J. H. Beijnen and G. Storm, *Mol Pharm*, 2011, **8**, 1002-1015.

55. G. J. Prud'homme and Y. Glinka, *Oncotarget*, 2012, **3**, 921-939.

56. J. R. Wild, C. A. Staton, K. Chapple and B. M. Corfe, *International journal of experimental pathology*, 2012, **93**, 81-103.

57. S. Tugues, S. Koch, L. Gualandi, X. Li and L. Claesson-Welsh, *Mol Aspects Med*, 2011, **32**, 88-111.

58. W. Cheng, D. Fu, Z. F. Wei, F. Xu, X. F. Xu, Y. H. Liu, J. P. Ge, F. Tian, C. H. Han, Z. Y. Zhang and L. M. Zhou, *Tumour Biol*, 2014, DOI: 10.1007/s13277-014-1806-3.
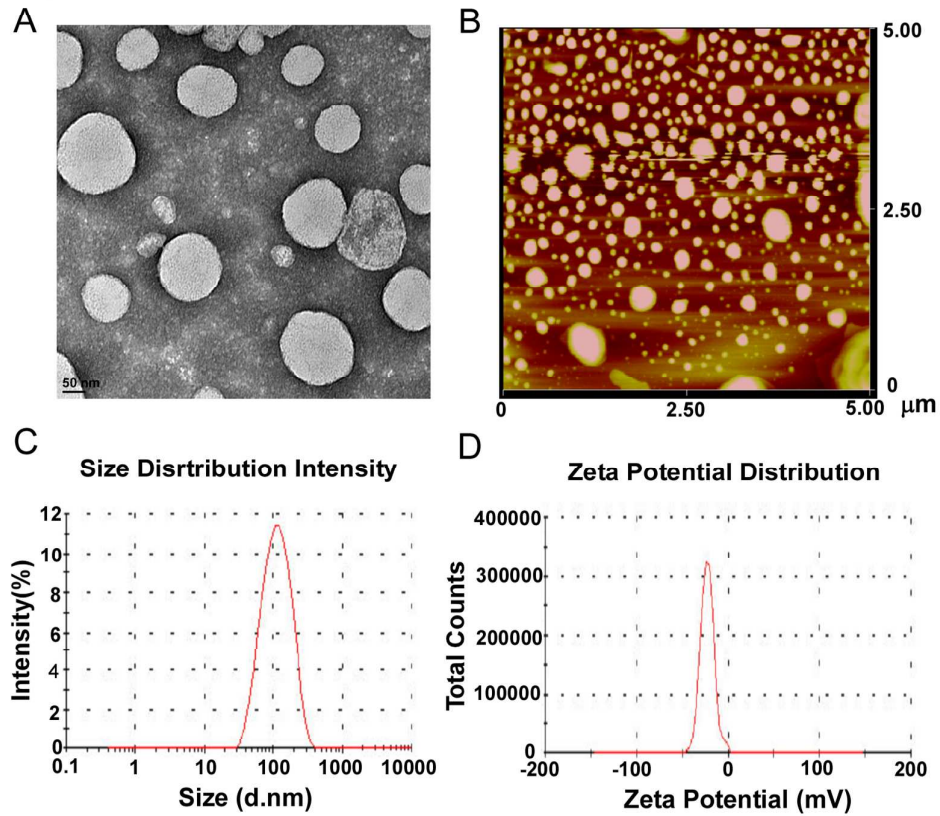
Fig.1

Fig. 1 Characterization of A7RC-LIPs. The morphology analysis of A7RC-LIPs was determined by Transmission electron microscopic (TEM) (A), Atomic force microscope AFM (B), Particle size (C) and Zeta potential (D).
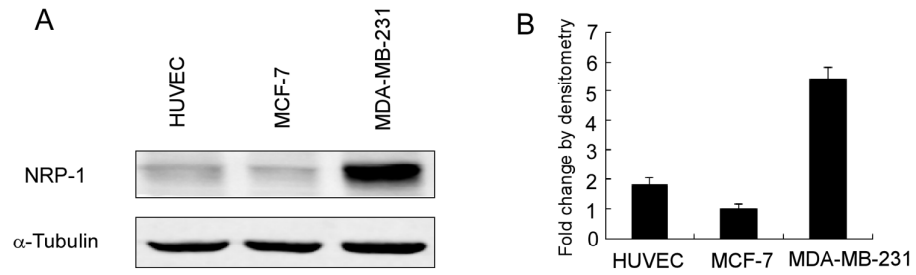
Fig.2

Fig. 2 Expression analysis of NRP-1 protein in breast cancer cell lines (MCF-7 and MDA-MB-231) and Human umbilical vein endothelial cells (HUVECs). A. The NRP-1 protein of HUVEC, MCF-7, and MDA-MB-231 cells was assayed by Western blot analysis. B. Fold change by densitometry was indicated.

Fig. 3
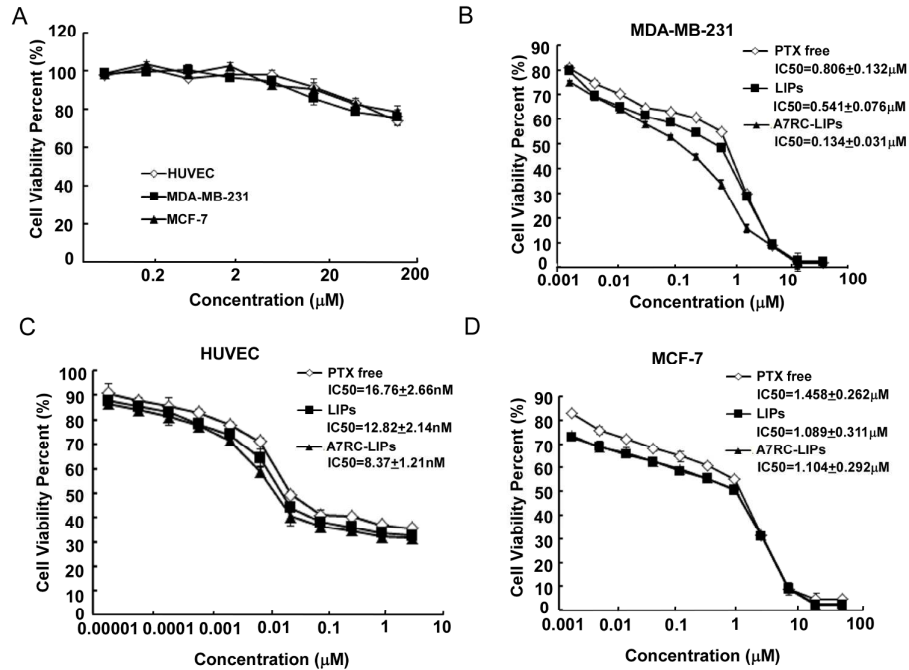
Fig. 3 Dose-response curves for A7RC and the cytotoxic effect of different paclitaxel formulations on cell viability. A. Dose-response curves of A7RC. The viability of each cell line (◊ represent HUVEC cell line, ▲represent MCF-7 cell line, and ■ represent MDA-MB-231 cell line) was plotted against the concentration of drug used in a 72 h treatment. B-D. The cytotoxic effects of various paclitaxel liposomes. The cytotoxicity on high, medium and low NRP-1 expression cells were plotted against the concentration of three paclitaxel formulations after 72h treatment. MDA-MB-231 cells (B), HUVECs (C), and MCF-7 (D) cells were assayed by MTT assay. ◊ represent free paclitaxel, ■represent LIPs, and ▲represent A7RC-LIPs. The IC50 values are shown. Each data point represents the geometric mean of at least three independent experiments, each performed at least in quadruplicates. Error bars represent values of S.D.
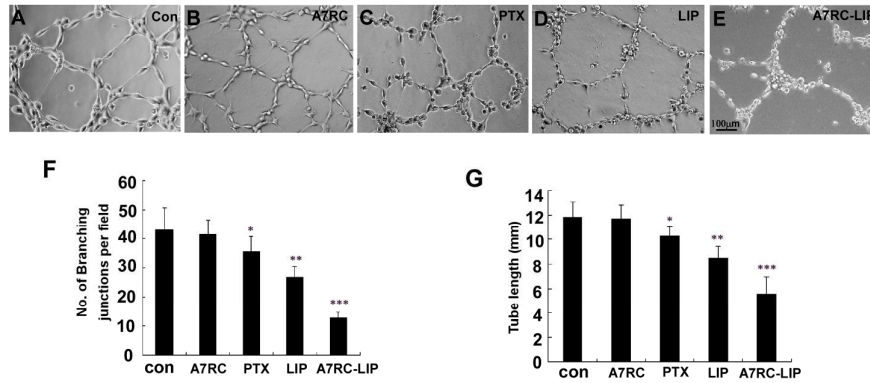
Fig.4

Fig. 4 The in vitro effects of A7RC and different paclitaxel formulations on HUVECs tube formation on matrigel. HUVECs were seeded on matrigel-coated 96-well plates at 3×10^3 cells/well in 1% FCS and 10ng/ml bFGF-containing medium in the absence (control)(A) or presence of 100μm A7RC (B) or 10nM free paclitaxel (C), 10nM LIPs (D), and 10nM A7RC-LIPs (E) for 24h. Representative image of tubes for each treatment is shown. Original magnifications: ×200. *Bar*, 100 μm. Three wells for each treatment were viewed, and the number of branching junctions (F) and length (G) of tubes formations were counted from 5 random microscopic fields per well at magnifications ×100. * represents *P*<0.05, ** represents *P*<0.01, *** represents *P*<0.001 each drug treated cells versus untreated control.
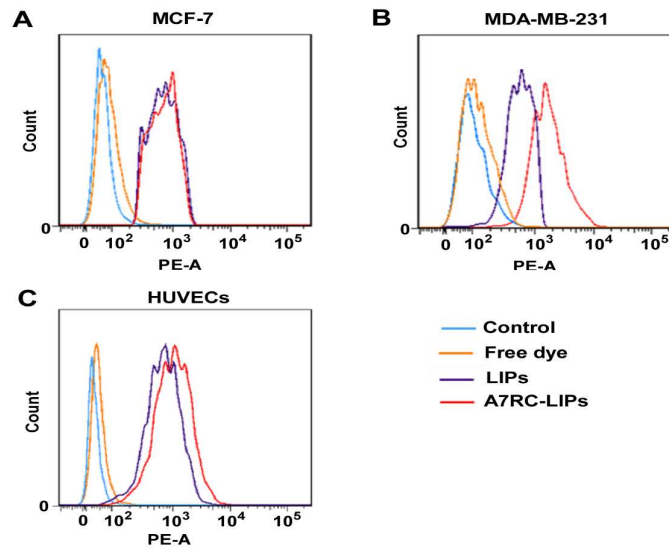
Fig 5

Fig. 5 Cellular uptake of LIPs and A7RC-LIPs in cells was monitored using flow cytometer. Shifting of the cellular uptake histogram peak for different preparations in MCF-7 cell line (A), MDA-MB-231 cell line (B) and HUVECs (C). Blue histogram represents control, orange histogram represents free Rho-labeled, purple histogram represents Rho-labeled LIPs, red histogram represents Rho-labeled A7RC-LIPs. Experiments were repeated at least three times and a representative experiment was shown.
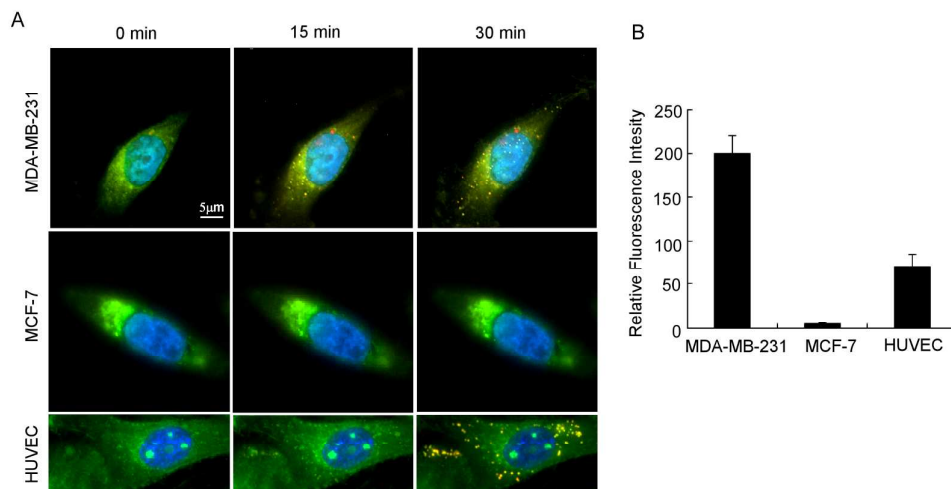
Fig.6

Fig. 6 Uptake and distribution of Rho-labeled A7RC-LIPs in different levels NRP-1 expressing breast cancer cells and HUVECs using time-lapse cell imaging analysis (A) and relative cellular fluorescence intensity analysis in each cells (B). A. Uptake and distribution of Rho-labeled A7RC-LIPs in high NRP-1 expressing MDA-MB-231 cells (the upper panel), low NRP-1 expressing MCF-7 cells (the middle panel), and HUVECs (the lower panel) from 0min to 30min. The cell cytomembrane was stained with Dio (green), cell nuclei stained with Hoechst 33258 (blue), and Rho-labeled A7RC-LIPs (Red), respectively. *Bar*, 5 *μ*m. B. Relative cellular fluorescence intensity analysis of Rho-labeled A7RC-LIPs in different cells. *Columns*, mean of triplicate determinations. *Bar*, S.D. Experiments were repeated at least three times and a representative experiment was shown.
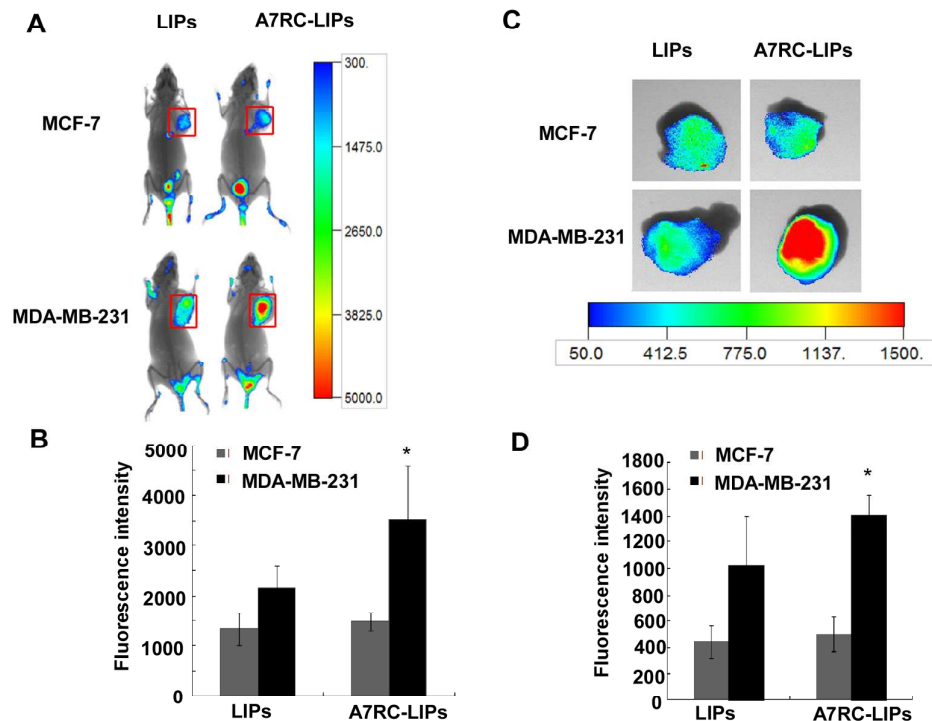
Fig.7

Fig.7 Tissue distribution of LIPs or A7RC-LIPs liposomal formulations (A and C) and relative fluorescence intensity analysis in each tumor tissue (B and D). A. *In vivo* images of whole body in mice bearing MCF-7 cells or MDA-MB-231 cells 4h after intravenous injection of each preparation with DiR-labeled LIPs or DiR-labeled A7RC-LIPs. B. Relative fluorescence intensity analysis of labeled LIPs or labeled A7RC-LIPs in tumor tissues of nude mice. C. *Ex vivo* images of MCF-7 cells or MDA-MB-231 cells xenografts from mice after intravenous injection of each preparation with DiR-labeled LIPs or DiR-labeled A7RC-LIPs. D. Relative fluorescence intensity analysis of labeled LIPs or labeled A7RC-LIPs in tumor tissues. The different pseudo colors in the photographs corresponded to the intensity of fluorescence signals, and the auto fluorescence of the controls was subtracted as the background. *Columns*, mean of triplicate determinations. *Bar*, S.D. Experiments were repeated at least three times and a representative experiment was shown. * represents $P<0.05$ relative fluorescence intensity of DiR-labeled A7RC-LIPs in tumor tissues versus that of DiR-labeled LIPs.
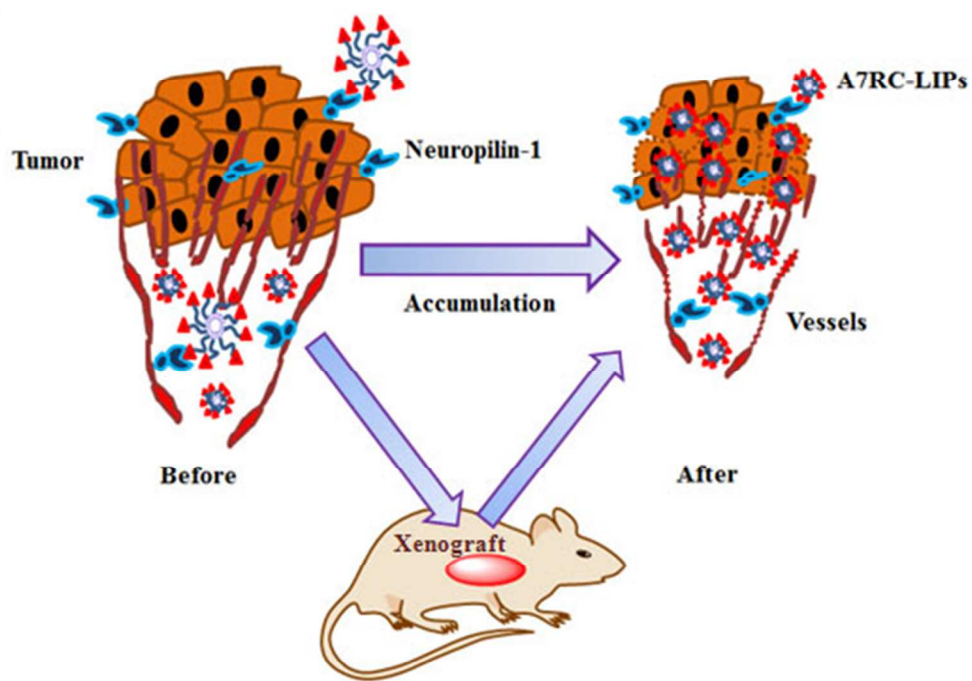
Graphic abstract: A7RC enhanced the accumulation of paclitaxel liposomes in Neuropilin-1 high expressing breast cancer mouse model and inhibited tumor growth and angiogenesis.